

Supervised Learning for Non-Sequential Data with the Canonical Polyadic Decomposition

Alexandros Haliassos*, Kriton Konstantinidis*, and Danilo P. Mandic, *Fellow, IEEE*

Abstract—There has recently been increasing interest, both theoretical and practical, in utilizing tensor networks for the analysis and design of machine learning systems. In particular, a framework has been proposed that can handle both dense data (e.g., standard regression or classification tasks) and sparse data (e.g., recommender systems), unlike support vector machines and traditional deep learning techniques. Namely, it can be interpreted as applying local feature mappings to the data and, through the outer product operator, modelling all interactions of functions of the features; the corresponding weights are represented as a tensor network for computational tractability. In this paper, we derive efficient prediction and learning algorithms for supervised learning with the Canonical Polyadic (CP) decomposition, including suitable regularization and initialization schemes. We empirically demonstrate that the CP-based model performs at least on par with the existing models based on the Tensor Train (TT) decomposition on standard non-sequential tasks, and better on MovieLens 100K. Furthermore, in contrast to previous works which applied two-dimensional local feature maps to the data, we generalize the framework to handle arbitrarily high-dimensional maps, in order to gain a powerful lever on the expressiveness of the model. In order to enhance its stability and generalization capabilities, we propose a normalized version of the feature maps. Our experiments show that this version leads to dramatic improvements over the unnormalized and/or two-dimensional maps, as well as to performance on non-sequential supervised learning tasks that compares favourably with popular models, including neural networks.

Index Terms—Tensor Networks, Supervised Learning, Canonical Polyadic Decomposition

I. INTRODUCTION

Tensor networks (TNs) have recently found various applications in supervised learning, owing to their interpretable, multilinear structure and ability to circumvent the curse of dimensionality by representing high-order tensors, i.e., multi-way arrays, by sets of interconnected lower-order tensors. For example, by establishing links between common TNs such as the Tensor Train (TT) [1] or Hierarchical Tucker (HT) [2], and deep learning architectures such as Recurrent [3], [4] or Convolutional Neural Networks [5], researchers were able to obtain new theoretical insights [6], [7], [8]. In addition, TNs have proven to be useful for the heavy compression of feedforward, convolutional, and recurrent networks without significant loss in performance [9], [10], [11].

This paper focuses on a related line of research, whereby TNs are employed for the design of scalable, interpretable, and general supervised learning models. More specifically,

a framework has been introduced [12], [13] that can be interpreted as applying local feature maps and subsequently the outer product operator to construct a rank-1 tensor that holds all possible feature interactions. The model prediction is given by the inner product of this tensor with a corresponding weight tensor. To render the computations tractable, the exponentially-large weight tensor is represented by a TN. By employing the TT and matrix TT formats, researchers were able to obtain competitive results on tasks including image recognition, recommender systems, and sequence-to-sequence learning [12], [13], [14].

The advantages of such models include:

- linear scaling with the dimensionality of the feature vectors and constant scaling with the training size (assuming mini-batch gradient descent is used for training), making them suitable for big data applications
- enhanced interpretability, due to the multi-linear nature of the model, that is lost with other state-of-the-art approaches such as neural networks and SVMs
- possession of the universal approximation property for large enough dimension of the local feature maps
- suitability for a wide range of supervised learning settings, including recommender systems, for which models such as neural networks and SVMs tend to underperform
- potential to derive novel machine learning models using multilinear algebra and to gain theoretical insights on existing approaches

Previous works have (either explicitly or implicitly) locally mapped the features to two-dimensional vectors, i.e., the *local dimension* was two. Being able to vary the local dimension plays a prominent role in the expressiveness of the models (they can only enjoy the universal approximation property if the local dimension is large enough) but leads to significant computational costs for learning algorithms that do not scale linearly with the local dimension, such as in [12], and results in instability or poor generalization depending on the feature map used.

In this work, we focus on the well-established Canonical Polyadic (CP) decomposition to represent the weight tensor and refer to this model as the *CP-based model* (naturally, we refer to the models based on TT as *TT-based*). The use of CP allows for simpler optimization algorithms, can lead to more parsimonious representations, and is insensitive to feature permutations, a desirable property for non-sequential data. We derive prediction and learning algorithms as well as initialization and regularization schemes that scale linearly with the dimensionality of the features and the local dimen-

The authors with an asterisk (*) contributed equally to this work.

All authors are with the Department of Electrical and Electronic Engineering, Imperial College London, London SW7 2AZ, U.K. (e-mails: {alexandros.haliassos14, k.konstantinidis19, d.mandic}@imperial.ac.uk)

sion. We show in Section IX that the model works at least on par with TT-based models on the non-sequential learning tasks that we experimented with and better on the MovieLens 100K recommender system dataset. A further contribution (that is agnostic to the type of decomposition used) is the extension of existing two-dimensional maps to generalized d -dimensional maps, which are able to model all interactions of features raised to powers of up to $d - 1$. To avoid erratic behavior of the learning procedure for high local dimension d , we propose to unit-normalize the vectors after mapping. Through experiments, we demonstrate that a higher d can dramatically enhance performance and that the algorithms remain stable even for $d > 100$. The performance boosts enjoyed by increasing d facilitated these models to achieve competitive results with popular models, including SVMs and feedforward neural networks. The CP-based model has been implemented as a custom layer in TensorFlow 2.0 to enable straightforward experimentation with various optimizers, regularizers, loss functions, etc.¹

The rest of the paper is organized as follows. First, we present the tensor preliminaries necessary to follow the technical part of the paper (Section II). Next, we describe the tensor network framework for supervised learning on which our algorithm is based (Section III). After a discussion on the interpretability of the model and its universal approximation property (Section IV), we present the derivations and algorithms for model prediction and learning (Section V). We then propose local feature maps for different settings (Section VI) and derive procedures for order regularization [13] (Section VII). We show how to initialize the model using the solution of a linear model trained on transformed features (Section VIII), and discuss results obtained during our experiments (Section IX). Finally, we provide links between the CP-based model and related works, discuss the advantages of our approach (Section X) and we conclude with potential future research directions (Section XI).

II. PRELIMINARIES

In this section, we present the notation and definitions necessary to follow the rest of the paper; for a more comprehensive review of TDs and TNs see [15], [16], [17].

A. Tensor Notation and Basic Operations

A real-valued tensor is a multidimensional array, which we denote in calligraphic typeface as $\mathcal{X} \in \mathbb{R}^{I_1 \times \dots \times I_N}$, where N is the order of the tensor, and I_n ($1 \leq n \leq N$) is the size of its n^{th} mode. Matrices (referenced with capital bold letters, e.g., $\mathbf{X} \in \mathbb{R}^{I_1 \times I_2}$) can be viewed as tensors with $N = 2$, vectors (given in lower-case bold letters, e.g., $\mathbf{x} \in \mathbb{R}^I$) with $N = 1$, and scalars (denoted by lower-case letters, e.g., $x \in \mathbb{R}$) with $N = 0$. A specific entry of a tensor $\mathcal{X} \in \mathbb{R}^{I_1 \times \dots \times I_N}$ is given by $x_{i_1, \dots, i_N} \in \mathbb{R}$. Moreover, we adopt a graphical notation, whereby a tensor is represented by a shape (e.g., a circle) with outgoing lines; the number of lines equals the order of the tensor (see [17] for more information on this graphical notation).

We employ the following conventions for basic linear/multilinear operations.

Definition 1 (Multi-Index). A multi-index (in reverse lexicographic ordering) is defined as $\overline{i_1 i_2 \dots i_N} = i_1 + (i_2 - 1)I_1 + (i_3 - 1)I_1 I_2 + \dots + (i_N - 1)I_1 \dots I_{N-1}$.

Definition 2 (Tensor Matricization). The mode- n matricization of a tensor $\mathcal{X} \in \mathbb{R}^{I_1 \times \dots \times I_N}$ reshapes the multidimensional array into a matrix $\mathbf{X}_{(n)} \in \mathbb{R}^{I_n \times I_1 I_2 \dots I_{n-1} I_{n+1} \dots I_N}$ with $(x_{(n)})_{i_n, \overline{i_1 \dots i_{n-1} i_{n+1} \dots i_N}} = x_{i_1, \dots, i_N}$.

Definition 3 (Outer Product). The outer product of two vectors $\mathbf{a} \in \mathbb{R}^I$ and $\mathbf{b} \in \mathbb{R}^J$ is given by $\mathbf{c} = \mathbf{a} \circ \mathbf{b} \in \mathbb{R}^{I \times J}$ with $c_{i,j} = a_i b_j$.

Definition 4 (Kronecker Product). The Kronecker product of two matrices $\mathbf{A} \in \mathbb{R}^{I \times J}$ and $\mathbf{B} \in \mathbb{R}^{K \times L}$ is denoted by $\mathbf{C} = \mathbf{A} \otimes \mathbf{B} \in \mathbb{R}^{I \times J \times K \times L}$ with $c_{(i-1)K+k, (j-1)L+l} = a_{i,j} b_{k,l}$.

Definition 5 (Khatri-Rao Product). The Khatri-Rao product of two matrices $\mathbf{A} = [\mathbf{a}_1, \dots, \mathbf{a}_R] \in \mathbb{R}^{I \times R}$ and $\mathbf{B} = [\mathbf{b}_1, \dots, \mathbf{b}_R] \in \mathbb{R}^{J \times R}$ is denoted by $\mathbf{C} = \mathbf{A} \odot \mathbf{B} \in \mathbb{R}^{I \times J \times R}$ with columns $\mathbf{c}_r = \mathbf{a}_r \otimes \mathbf{b}_r$, $1 \leq r \leq R$.

Definition 6 (Hadamard Product). The Hadamard product of two N^{th} -order tensors $\mathcal{A} \in \mathbb{R}^{I_1 \times \dots \times I_N}$ and $\mathcal{B} \in \mathbb{R}^{I_1 \times \dots \times I_N}$ is denoted by $\mathcal{C} = \mathcal{A} \otimes \mathcal{B} \in \mathbb{R}^{I_1 \times \dots \times I_N}$ with $c_{i_1, \dots, i_N} = a_{i_1, \dots, i_N} b_{i_1, \dots, i_N}$.

Definition 7 (Tensor Contraction). The contraction of an N^{th} -order tensor $\mathcal{A} \in \mathbb{R}^{I_1 \times \dots \times I_N}$ and an M^{th} -order tensor $\mathcal{B} \in \mathbb{R}^{J_1 \times \dots \times J_M}$ over the n^{th} and m^{th} modes respectively, where $I_n = J_m$, results in an $(N + M - 2)^{\text{th}}$ -order tensor with entries $c_{i_1, \dots, i_{n-1}, i_{n+1}, \dots, i_N, j_1, \dots, j_{m-1}, j_{m+1}, \dots, j_M} = \sum_{i_n=1}^{I_n} a_{i_1, \dots, i_{n-1}, i_n, i_{n+1}, \dots, i_N} b_{j_1, \dots, j_{m-1}, i_n, j_{m+1}, \dots, j_M}$. Contraction is illustrated elegantly in the graphical notation simply by connecting the corresponding lines of the tensors.

Definition 8 (Inner Product of Tensors). The inner product of two N^{th} -order tensors $\mathcal{A} \in \mathbb{R}^{I_1 \times \dots \times I_N}$ and $\mathcal{B} \in \mathbb{R}^{I_1 \times \dots \times I_N}$ is denoted by $c = \langle \mathcal{A}, \mathcal{B} \rangle \in \mathbb{R}$ with $c = \sum_{i_1, \dots, i_N} a_{i_1, \dots, i_N} b_{i_1, \dots, i_N}$.

A property (see Appendix A for proof) that we use in this paper is

$$\begin{aligned} & \left(\mathbf{A}^{(1)} \odot \dots \odot \mathbf{A}^{(N)} \right)^T \left(\mathbf{B}^{(1)} \odot \dots \odot \mathbf{B}^{(N)} \right) \\ &= \mathbf{A}^{(1)T} \mathbf{B}^{(1)} \otimes \dots \otimes \mathbf{A}^{(N)T} \mathbf{B}^{(N)} \\ &= \bigotimes_{k=1}^N \mathbf{A}^{(k)T} \mathbf{B}^{(k)}, \end{aligned} \quad (1)$$

where $\mathbf{A}^{(k)} \in \mathbb{R}^{I_k \times J}$ and $\mathbf{B}^{(k)} \in \mathbb{R}^{I_k \times L}$.

B. Tensor Train and Canonical Polyadic Decompositions

1) *Tensor Networks:* A TN provides an efficient representation of a tensor as a set of lower-order tensors which are contracted over certain modes. The relatively low order of the tensors and their sparse interconnections allow the avoidance of the curse of dimensionality as the size of the representation tends to scale linearly with the tensor order (rather than exponentially).

¹https://github.com/KritonKonstantinidis/CPD_Supervised_Learning

2) *Tensor Train Decomposition*: A tensor $\mathcal{X} \in \mathbb{R}^{I_1 \times \dots \times I_N}$ can be represented in the Tensor Train (TT) format as

$$\mathcal{X} = \mathcal{G}^{(1)} \times^1 \dots \times^1 \mathcal{G}^{(N)}, \quad (2)$$

where $\mathcal{G}^{(n)} \in \mathbb{R}^{R_{n-1} \times I_n \times R_n}$, $R_0 = R_N = 1$, are the TT cores, and $\mathcal{G}^{(n)} \times^1 \mathcal{G}^{(n+1)}$ denotes contraction over the last mode of $\mathcal{G}^{(n)}$ and first mode of $\mathcal{G}^{(n+1)}$. The TT rank is given by the dimensions of the contracted modes, i.e., TT rank = $\{R_1, \dots, R_{N-1}\}$. The TT format is depicted on the left panel of Fig. 1.

3) *Canonical Polyadic Decomposition*: The Canonical Polyadic (CP) decomposition [18], [19] expresses a tensor $\mathcal{X} \in \mathbb{R}^{I_1 \times \dots \times I_N}$ as a sum of outer products of vectors (i.e., rank-1 terms):

$$\begin{aligned} \mathcal{X} &= \sum_{r=1}^R \mathbf{a}_r^{(1)} \circ \dots \circ \mathbf{a}_r^{(N)} \\ &= \sum_{r=1}^R \bigcirc_{k=1}^N \mathbf{a}_r^{(k)}, \end{aligned} \quad (3)$$

where R is the CP rank of the tensor (this is equal to the standard matrix rank when $N = 2$). We can collect these vectors into N factor matrices $\mathbf{A}^{(n)} = [\mathbf{a}_1^{(n)}, \dots, \mathbf{a}_R^{(n)}] \in \mathbb{R}^{I_n \times R}$, ($1 \leq n \leq N$), in which case the CP decomposition can be expressed as a contraction of the identity tensor $\mathcal{I} \in \mathbb{R}^{I_1 \times \dots \times I_N}$ (all ones on the super-diagonal) with all factor matrices. This view allows the CP decomposition to be formulated as a TN, as is shown on the right panel in Fig. 1.

The entries of the CPD can be expressed as

$$\begin{aligned} x_{i_1, \dots, i_N} &= \sum_{r=1}^R a_{i_1, r}^{(1)} a_{i_2, r}^{(2)} \dots a_{i_N, r}^{(N)} \\ &= \left(\bigcirc_{k=1}^N \hat{\mathbf{a}}_{i_k}^{(k)} \right) \mathbf{1}, \end{aligned} \quad (4)$$

where $\hat{\mathbf{a}}_j^{(n)}$ denotes the j^{th} row of the n^{th} factor matrix, and $\mathbf{1} = [1, \dots, 1]^T \in \mathbb{R}^R$.

Upon matricization of \mathcal{X} we obtain

$$\begin{aligned} \mathbf{X}_{(n)} &= \mathbf{A}^{(n)} \left(\mathbf{A}^{(N)} \odot \dots \odot \mathbf{A}^{(n+1)} \odot \mathbf{A}^{(n-1)} \right. \\ &\quad \left. \odot \dots \odot \mathbf{A}^{(1)} \right)^T \\ &= \mathbf{A}^{(n)} \left(\bigcirc_{\substack{k=N \\ k \neq n}}^1 \mathbf{A}^{(k)} \right)^T. \end{aligned} \quad (5)$$

Furthermore, its vectorization is expressed as

$$\text{vec}(\mathcal{X}) = \left(\bigcirc_{k=N}^1 \mathbf{A}^{(k)} \right) \mathbf{1}. \quad (6)$$

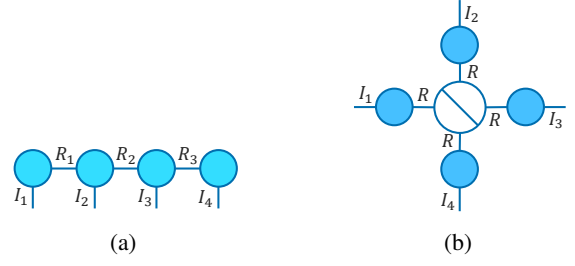


Fig. 1: Tensor Network notation of (a) Tensor Train and (b) Canonical Polyadic decomposition. A circle with a diagonal line denotes a super-diagonal tensor, in this case the identity.

III. TENSOR NETWORK FRAMEWORK FOR SUPERVISED LEARNING

Consider a local feature mapping $\phi: \mathbb{R} \rightarrow \mathbb{R}^d$ applied to every feature x_n , where d is referred to as the *local dimension* of the mapping. The choice of the feature map is flexible and application-dependent. We take the outer product between the mapped vectors to obtain

$$\Phi(\mathbf{x}) = \bigcirc_{k=1}^N \phi(x_k) \in \mathbb{R}^{d^N}. \quad (7)$$

Note that \mathbb{R}^{d^N} is shorthand for $\mathbb{R}^{\overbrace{d \times \dots \times d}^{N \text{ times}}}$. The prediction produced by the model for one output (e.g., single-target regression or binary classification) is given by

$$f(\mathbf{x}) = \langle \Phi(\mathbf{x}), \mathcal{W} \rangle, \quad (8)$$

where $\mathcal{W} \in \mathbb{R}^{d^N}$ is the *weight tensor*, holding all model coefficients. Note that in the case of multi-target regression or multi-class classification with L labels, the model is composed of L different weight tensors \mathcal{W}^l ($1 \leq l \leq L$). For a graphical representation in tensor network notation, see Figure 2.

Example 1. Consider the map $\phi(x_n) = [1, x_n]^T$. Then, for number of features $N = 3$, we have $\Phi(\mathbf{x}) \in \mathbb{R}^{2 \times 2 \times 2}$ and

$$\begin{aligned} f(\mathbf{x}) &= w_{1,1,1} + w_{2,1,1}x_1 + w_{1,2,1}x_2 + w_{1,1,2}x_3 + w_{2,2,1}x_1x_2 \\ &\quad + w_{2,1,2}x_1x_3 + w_{1,2,2}x_2x_3 + w_{2,2,2}x_1x_2x_3. \end{aligned} \quad (9)$$

Thus, the model in this case captures all combinations of distinct features.

The size of the weight tensor \mathcal{W} scales exponentially with the number of features and is therefore computationally prohibitive to learn. For this reason, \mathcal{W} is represented as a tensor network with exponentially lower number of parameters. In this work, we represent \mathcal{W} in the CP format, which is insensitive to the ordering of the features (see X-A). Although this is also true for the Tucker decomposition [15], using the Tucker format entails exponential scaling with the number of features. Also, the Tucker decomposition is achieved through a core tensor whose modes typically have dimensions smaller than those of the original tensor, rendering them unsuitable for weight tensors with dimensions 2 across all modes, such as in Example 1.

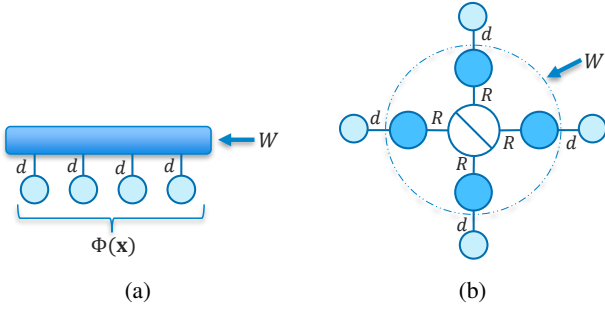


Fig. 2: Model prediction (a) without decomposition and (b) with CP decomposition of \mathcal{W} .

IV. CP-BASED MODEL

A. Model Prediction and Interpretability

It is important to notice that the model prediction can be expressed in terms of the rows of the CP model's factor matrices and the corresponding elements of the feature mapping:

$$f(\mathbf{x}) = \sum_{i_1, \dots, i_N} w_{i_1, \dots, i_N} \prod_{k=1}^N \phi(x_k)_{i_k} \quad (10)$$

$$= \sum_{i_1, \dots, i_N} \left(\bigotimes_{k=1}^N \hat{\mathbf{a}}_{i_k}^{(k)} \right) \mathbf{1} \prod_{k=1}^N \phi(x_k)_{i_k}. \quad (11)$$

In other words, the coefficient for each (transformed) feature interaction can be readily obtained after training simply by performing a Hadamard product of the corresponding row vectors of the learned factor matrices and then summing over all entries of the resulting vector. This provides enhanced interpretability over SVMs or deep learning techniques, as the importance of a given feature interaction can be observed in $\mathcal{O}(NRd)$ time.

Example 2. Consider again the mapping $\phi(x_n) = [1, x_n]^T$ with $N = 3$. Then, the coefficient for $x_1 x_3$ would be obtained by finding the Hadamard product of $\hat{\mathbf{a}}_2^{(1)}$, $\hat{\mathbf{a}}_1^{(2)}$, and $\hat{\mathbf{a}}_2^{(3)}$, and then summing over the entries.

B. Universal Approximation Property

It is known that the TN framework discussed in Section III can approximate any function with any approximation error, as long as d is large enough [6]. Since there always exists a CP rank for which a tensor can be exactly decomposed in its CP form, the proposed model satisfies the universal approximation property. This highlights the importance of using a higher d for the feature map.

Example 3. Consider $\phi(x_n) = [1, x_n, x_n^2, \dots, x_n^{(d-1)}]^T$; then, by varying d and R , the model can capture any polynomial function. By Stone-Weierstrass theorem [20], there exist d and R such that the model can approximate any continuous function on compact subsets of \mathbb{R}^N .

V. PREDICTION AND LEARNING ALGORITHMS

This section is concerned with efficient algorithms for the model predictions as well as for learning the model parameters. The mathematical derivations of our algorithms were

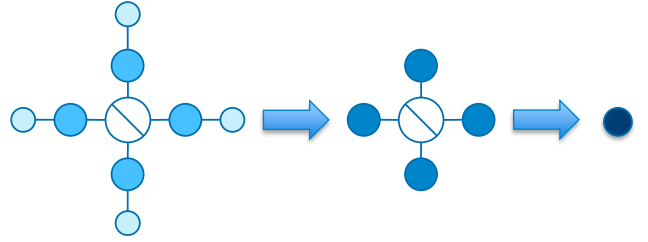


Fig. 3: Model prediction in the graphical TN notation. First arrow denotes matrix-vector multiplications for all factor matrices and second arrow sum of Hadamard products of all resulting vectors.

included for rigor; the reader can refer to the graphical notation to gain intuition on the underlying algorithms.

A. Prediction Algorithm

Given the factor matrices $\mathbf{A}^{(n)}$ and the maps $\phi(x_n)$ ($1 \leq n \leq N$), there are various ways of obtaining the model predictions, some of which are dramatically more computationally efficient than others. For example, implementing (8) directly yields a procedure that scales exponentially with N .

We now derive an efficient procedure for computing the prediction. The prediction can be expressed as

$$\begin{aligned} f(\mathbf{x}) &= \langle \Phi(\mathbf{x}), \mathcal{W} \rangle \\ &= \langle \text{vec}(\Phi(\mathbf{x})), \text{vec}(\mathcal{W}) \rangle \\ &= \text{vec}(\Phi(\mathbf{x}))^T \text{vec}(\mathcal{W}) \\ &= \text{vec} \left(\bigcirc_{k=1}^N \phi(x_k) \right)^T \text{vec} \left(\sum_{r=1}^R \bigcirc_{k=1}^N \mathbf{a}_r^{(k)} \right) \\ &= \left(\bigcirc_{k=N}^1 \phi(x_k) \right)^T \left(\bigcirc_{k=N}^1 \mathbf{A}^{(k)} \right) \mathbf{1} \\ &= \left(\bigotimes_{k=1}^N \phi(x_k)^T \mathbf{A}^{(k)} \right) \mathbf{1}. \end{aligned} \quad (12)$$

The corresponding procedure is given in Algorithm 1, the complexity of which is $\mathcal{O}(NRd)$.² The algorithm can be visualized using the graphical TN notation (see Fig. 3). Notice that obtaining the model predictions amounts to contracting the TN in Fig. 2.

B. Learning Algorithm

In order to learn the model parameters (i.e., factor matrices) using an approach based on first-order derivatives (e.g., stochastic gradient descent, ADAM [21], etc.) we need to obtain the partial derivative of the prediction with respect to each factor matrix (the desired gradient can subsequently be computed using the chain rule). Alternatively, one can employ automatic differentiation, for example in Keras [22], and specify only the forward pass (i.e., Algorithm 1).

²Throughout the paper we give the asymptotic complexity of the algorithms, assuming that each operation is executed in sequence. The methods are, however, highly amenable to parallelization, and they can be implemented in TensorFlow very efficiently.

Algorithm 1: Model Prediction

Input: Data point $\mathbf{x} \in \mathbb{R}^N$ and factor matrices $\mathbf{A}^{(n)} \in \mathbb{R}^{d \times R}$, $1 \leq n \leq N$
Output: Prediction $\hat{y} \in \mathbb{R}$
begin
 // Construct feature maps $\phi(x_n) \in \mathbb{R}^{d \times 1}$ for $1 \leq n \leq N$
 $\mathbf{p} = \mathbf{1}^T \in \mathbb{R}^{1 \times R}$ // Initialize (row) vector of ones
for $n = 1, \dots, N$ **do**
 | $\mathbf{p} \leftarrow \mathbf{p} \circledast \phi(x_n)^T \mathbf{A}^{(n)}$
end
 $\hat{y} = \text{sum}(\mathbf{p})$ // Sum entries of \mathbf{p}
end

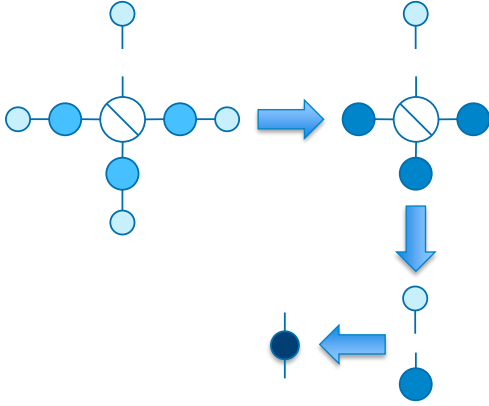


Fig. 4: Partial derivative of prediction w.r.t. a given factor matrix. First arrow denotes matrix-vector multiplications for all but one factor matrices, second arrow Hadamard product of the resulting vectors, and third arrow outer product of the remaining vectors.

With view to deriving the partial derivative analytically, consider the following expression of the prediction, which uses the mode- n matricization of the tensors:

$$\begin{aligned}
 f(\mathbf{x}) &= \langle \Phi(\mathbf{x}), \mathcal{W} \rangle \\
 &= \langle \Phi(\mathbf{x})_{(n)}, \mathbf{W}_{(n)} \rangle \\
 &= \text{Tr} \left(\Phi(\mathbf{x})_{(n)}^T \mathbf{W}_{(n)} \right) \\
 &= \text{Tr} \left(\left(\begin{array}{c} 1 \\ \circ \\ \phi(x_k) \\ \circ \\ \mathbf{A}^{(n)} \end{array} \right) \phi(x_n)^T \mathbf{A}^{(n)} \left(\begin{array}{c} 1 \\ \circ \\ \mathbf{A}^{(k)} \\ \circ \\ \phi(x_k) \end{array} \right)^T \right) \\
 &= \text{Tr} \left(\mathbf{A}^{(n)} \left(\begin{array}{c} 1 \\ \circ \\ \mathbf{A}^{(k)} \\ \circ \\ \phi(x_k) \end{array} \right)^T \left(\begin{array}{c} 1 \\ \circ \\ \phi(x_k) \\ \circ \\ \mathbf{A}^{(k)} \end{array} \right) \phi(x_n)^T \right) \\
 &= \text{Tr} \left(\mathbf{A}^{(n)} \left(\begin{array}{c} N \\ \circ \\ \mathbf{A}^{(k)T} \phi(x_k) \\ \circ \\ \phi(x_n)^T \end{array} \right) \right), \quad (13)
 \end{aligned}$$

where $\text{Tr}(\cdot)$ denotes the trace operator and we have used its cyclic property.

The partial derivative of the prediction w.r.t. the n^{th} factor matrix is then given by

$$\frac{\partial f(\mathbf{x})}{\partial \mathbf{A}^{(n)}} = \phi(x_n) \left(\begin{array}{c} N \\ \circ \\ \phi(x_k)^T \mathbf{A}^{(k)} \\ \circ \\ \phi(x_n) \end{array} \right), \quad (14)$$

where we have used the well-known matrix calculus identity

$$\frac{\partial}{\partial \mathbf{X}} \text{Tr}(\mathbf{X}\mathbf{W}) = \mathbf{W}^T. \quad (15)$$

In graphical notation, the corresponding procedure is depicted in Fig. 4. Notice that naively implementing (14) leads to a computational complexity of $\mathcal{O}(NRd)$ for obtaining the partial derivative w.r.t. each factor matrix and thus of $\mathcal{O}(N^2Rd)$ w.r.t. to all factors. The quadratic scaling with N is due to a repetition of the same matrix-vector products as we take the derivative w.r.t. different factors, which can be obviated by storing these products. This leads to Algorithm 2, which has a complexity of $\mathcal{O}(NRd)$.

Algorithm 2: Partial Derivative of Prediction

Input: Data point $\mathbf{x} \in \mathbb{R}^N$ and factor matrices $\mathbf{A}^{(n)} \in \mathbb{R}^{d \times R}$, $1 \leq n \leq N$
Output: Partial derivative $\frac{\partial f(\mathbf{x})}{\partial \mathbf{A}^{(n)}} \in \mathbb{R}^{d \times R}$ for $1 \leq n \leq N$
begin
 // Construct feature maps $\phi(x_n) \in \mathbb{R}^{d \times 1}$ for $1 \leq n \leq N$
 $\mathbf{p} = \mathbf{1}^T \in \mathbb{R}^{1 \times R}$ // Initialize (row) vector of ones
for $n = 1, \dots, N$ **do**
 | $\mathbf{m}_n = \phi(x_n)^T \mathbf{A}^{(n)} \in \mathbb{R}^{1 \times R}$ // Store matrix-vector products
 | $\mathbf{p} \leftarrow \mathbf{p} \circledast \mathbf{m}_n$ // Store Hadamard products
end
for $n = 1, \dots, N$ **do**
 | $\mathbf{d} = \mathbf{p} \circledast \mathbf{m}_n \in \mathbb{R}^{1 \times R}$ // Divide element-wise
 | $\frac{\partial f(\mathbf{x})}{\partial \mathbf{A}^{(n)}} = \phi(x_n) \mathbf{d}$
end
end

VI. LOCAL FEATURE MAPPINGS

A. Polynomial Mapping

In this paper, we focus on features maps of the form

$$\phi_d(x_n) = [1, x_n, x_n^2, \dots, x_n^{(d-1)}]^T, \quad (16)$$

which is an extension to the map used in [13], i.e., $\phi_{\text{EM}}(x_n) = [1, x_n]^T$. We include the subscript in (16) to emphasize the dependence on d . The map given in (16) contains the linear model (see Section VIII), does not restrict the set of feature standardization techniques that can be employed (see Remark 1), and allows the straightforward modification of d , so that we have an additional lever (aside from the rank R) on the expressiveness of the model.

B. Normalized Polynomial Mapping

At high enough d , (16) causes instability in the training process and very high overfitting, especially in the presence of outliers. We found that normalizing the resulting vector to unit length enables the use of very high d , even $d > 100$, and also performs significantly better in the experiments that we conducted (see Section IX).

The map can be expressed as

$$\hat{\phi}_d(x_n) = \frac{1}{\sqrt{\sum_{k=0}^{d-1} x_n^{2k}}} [1, x_n, x_n^2, \dots, x_n^{(d-1)}]^T. \quad (17)$$

Note that, due to the dependence of the denominator on the feature values, there no longer exists a bias term. One could include a 1 at the start of the vector in (17), or simply fit a bias with an independent parameter, though we achieved best performance in our experiments simply using (17).

The data are pre-processed by standardizing the features; otherwise, increasing d would quickly risk numerical overflow. We found in our experiments that a standard deviation of 1 (and mean of 0) worked well. These parameters imply that almost all feature values range between -3 and 3 after this preprocessing step, and so even $d = 75$ does not cause overflow for 32-bit single-precision floating-point representation (one can use double-point precision for extremely high d). Furthermore, the entries of the vector in (17) either decrease exponentially with the index if the standardized feature values are between -1 and 1 or increase exponentially otherwise. Hence, only a few of the vector entries have a non-negligible impact on the prediction. This seems to have a positive effect on both the training and validation errors, since standardizing the powers of x_n before vector normalization led to significantly worse results.

A possible reason for the stability of the algorithm and smoothness of the learning curves when the normalized map is used, even when the data contain outliers, is that the norms of the vectors after the matrix-vector multiplications in the prediction (see Fig. 3) remain bounded within the same range at each iteration:

$$\sigma_{\min} \leq \left\| \phi(x_n)^T \mathbf{A}^{(n)} \right\| \leq \left\| \mathbf{A}^{(n)} \right\|, \quad (18)$$

where σ_{\min} denotes the smallest singular value of $\mathbf{A}^{(n)}$. Notice that the bound does not depend on the data.

C. Mapping for Categorical Data

An advantage of this framework for supervised learning is its ability to handle categorical features after they have been one-hot encoded. Although it is possible to concatenate all binary one-hot features into a large feature vector and allocate a factor matrix to each feature, thereby enabling the use of (16) with $d = 2$, this would unnecessarily model interactions between one-hot features belonging to the same categorical variable. For this reason, the feature map used for categorical data is instead

$$\phi(x_n) = \left[1, \mathbf{v}_n^T \right]^T, \quad (19)$$

where $\mathbf{v}_n \in \mathbb{R}^{K_n}$ is the one-hot-encoded representation of the n^{th} categorical feature, and K_n is the number of values that the feature can assume.

Remark 1. A feature map that was inspired by quantum physics and has been used in [12], [23] for object recognition tasks is $\phi(x_n) = \left[\cos\left(\frac{\pi}{2}x_n\right), \sin\left(\frac{\pi}{2}x_n\right) \right]^T$. A potential issue of this map for other types of tasks is that \cos and \sin are one-to-one functions only if their domains are restricted; thus, if the input features are unbounded (i.e., there are no pre-defined minimum and maximum values), one can only apply Min-Max scaling (and not other standardization techniques) to the features as a preprocessing step. Although pixel values are bounded (typically from 0 to 255), this is not normally the case for other data types. This is especially problematic when there exist outliers, as, in that case, Min-Max scaling can result in extremely small standard deviations for the scaled features, adversely impacting performance.

VII. REGULARIZATION

Although the CP decomposition itself provides strong regularization for small rank, we can potentially improve the performance by guiding the training algorithm to hypotheses that are more likely to generalize well to unseen data. Standard regularizers, such as L1 and L2, do not differentiate between the coefficients for different feature interactions in (11). This is potentially suboptimal when using the polynomial or categorical mappings, because we might want to limit the coefficients of the higher-order terms relatively more. *Order regularization* [13] addresses this by penalizing large coefficients for higher-order terms more than for lower-order ones. In this section, we show how to apply order regularization to our model.

The penalty for order regularization is given by $\langle \mathcal{B} \otimes \mathcal{W}, \mathcal{B} \otimes \mathcal{W} \rangle$, where $\mathcal{B} = \bigcirc_{k=1}^N \mathbf{b}$ for a user-defined vector \mathbf{b} . In the case of polynomial functions, one choice is $\mathbf{b} = [1, \beta, \beta^2, \dots, \beta^{d-1}]^T$ with $\beta > 1$: the coefficients of the higher-order terms are multiplied by a higher power of β in the computation of the penalty function, and the factor matrices are adjusted in such a way as to shrink these coefficients relatively more. In the case of categorical feature mapping, $\mathbf{b} = [1, \beta, \beta, \dots, \beta]^T$ is more suitable, since all binary, one-hot features should be treated equally.

A. Computation of the Order Regularization Penalty

Notice that

$$\begin{aligned} \mathcal{B} \otimes \mathcal{W} &= \left(\bigcirc_{k=1}^N \mathbf{b} \right) \otimes \left(\sum_{r=1}^R \bigcirc_{k=1}^N \mathbf{a}_r^{(k)} \right) \\ &= \sum_{r=1}^R \bigcirc_{k=1}^N \left(\mathbf{a}_r^{(k)} \otimes \mathbf{b} \right). \end{aligned} \quad (20)$$

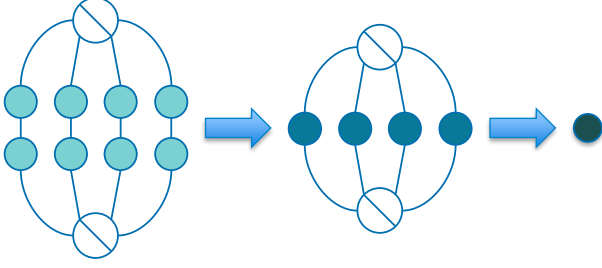


Fig. 5: Order regularization penalty in graphical TN notation for $N = 4$. First arrow denotes matrix-matrix multiplications for all factor matrices and second arrow sum of Hadamard products of all resulting matrices. Note that the matrices in the left-most TN are the result of the Hadamard products $\mathbf{A}^{(n)} \circledast \mathbf{B}$.

Now, let $\mathbf{B} = [\mathbf{b}, \dots, \mathbf{b}] \in \mathbb{R}^{d \times R}$ and $\mathbf{Y}^{(n)} = \mathbf{A}^{(n)} \circledast \mathbf{B}$. The penalty can be re-written as

$$\begin{aligned} P(\mathcal{B}, \mathcal{W}) &= \text{vec}(\mathcal{B} \circledast \mathcal{W})^T \text{vec}(\mathcal{B} \circledast \mathcal{W}) \\ &= \mathbf{1}^T \left(\begin{array}{c} \mathbf{1} \\ \circledast \\ \mathbf{Y}^{(k)} \\ k=N \end{array} \right)^T \left(\begin{array}{c} \mathbf{1} \\ \circledast \\ \mathbf{Y}^{(k)} \\ k=N \end{array} \right) \mathbf{1} \\ &= \mathbf{1}^T \left(\begin{array}{c} N \\ \circledast \\ \mathbf{Y}^{(k)T} \mathbf{Y}^{(k)} \\ k=1 \end{array} \right) \mathbf{1}. \end{aligned} \quad (21)$$

The procedure for computing the regularization penalty is given in Algorithm 3 and depicted graphically in Fig. 5. The algorithm has a computational cost of $\mathcal{O}(NR^2d)$, so the training procedure scales quadratically with R with order regularization (rather than linearly).

Algorithm 3: Order Regularization Penalty

Input: Factor matrices $\mathbf{A}^{(n)} \in \mathbb{R}^{d \times R}$, $1 \leq n \leq N$, order regularization parameter $\mathbf{b} \in \mathbb{R}^{d \times 1}$, and regularization constant $\alpha \in \mathbb{R}$

Output: Penalty $P \in \mathbb{R}$

begin

$\mathbf{B} = [\mathbf{b}, \dots, \mathbf{b}]^T \in \mathbb{R}^{d \times R}$

$\mathbf{P} = [\mathbf{1}, \dots, \mathbf{1}]^T \in \mathbb{R}^{R \times R}$ // Initialize all-ones matrix

for $n = 1, \dots, N$ **do**

$\mathbf{P} \leftarrow \mathbf{P} \circledast \left(\left(\mathbf{A}^{(n)} \circledast \mathbf{B} \right)^T \left(\mathbf{A}^{(n)} \circledast \mathbf{B} \right) \right)$

end

$P = \alpha * \text{sum}(\mathbf{P})$ // Sum entries of \mathbf{P}

end

B. Partial Derivative of the Order Regularization Penalty

The partial derivative of the order regularization penalty w.r.t. each factor matrix can be found by first expressing the

penalty in the following way:

$$\begin{aligned} P &= \left\langle \left(\mathbf{B}^{(n)} \circledast \mathbf{W}^{(n)} \right), \left(\mathbf{B}^{(n)} \circledast \mathbf{W}^{(n)} \right) \right\rangle \\ &= \text{Tr} \left(\left(\mathbf{B}^{(n)} \circledast \mathbf{W}^{(n)} \right)^T \left(\mathbf{B}^{(n)} \circledast \mathbf{W}^{(n)} \right) \right) \\ &= \text{Tr} \left(\left(\begin{array}{c} \mathbf{1} \\ \circledast \\ \mathbf{Y}^{(k)} \\ k=N \\ k \neq n \end{array} \right) \mathbf{Y}^{(n)T} \mathbf{Y}^{(n)} \left(\begin{array}{c} \mathbf{1} \\ \circledast \\ \mathbf{Y}^{(k)} \\ k=N \\ k \neq n \end{array} \right)^T \right) \\ &= \text{Tr} \left(\mathbf{Y}^{(n)} \left(\begin{array}{c} \mathbf{1} \\ \circledast \\ \mathbf{Y}^{(k)} \\ k=N \\ k \neq n \end{array} \right)^T \left(\begin{array}{c} \mathbf{1} \\ \circledast \\ \mathbf{Y}^{(k)} \\ k=N \\ k \neq n \end{array} \right) \mathbf{Y}^{(n)T} \right) \\ &= \text{Tr} \left(\mathbf{Y}^{(n)} \left(\begin{array}{c} N \\ \circledast \\ \mathbf{Y}^{(k)T} \mathbf{Y}^{(k)} \\ k=1 \\ k \neq n \end{array} \right) \mathbf{Y}^{(n)T} \right). \end{aligned} \quad (22)$$

Then, using the identity (see Appendix B for proof)

$$\begin{aligned} \frac{\partial}{\partial \mathbf{X}} \text{Tr} \left((\mathbf{X} \circledast \mathbf{W}) \mathbf{Z} (\mathbf{X} \circledast \mathbf{W})^T \right) &= \\ &= \mathbf{W} \circledast \left((\mathbf{X} \circledast \mathbf{W}) (\mathbf{Z} + \mathbf{Z}^T) \right) \end{aligned} \quad (23)$$

we obtain (notice that in this case $\mathbf{Z} = \mathbf{Z}^T$)

$$\frac{\partial P}{\partial \mathbf{A}^{(n)}} = 2\mathbf{B} \circledast \left(\mathbf{Y}^{(n)} \left(\begin{array}{c} N \\ \circledast \\ \mathbf{Y}^{(k)T} \mathbf{Y}^{(k)} \\ k=1 \\ k \neq n \end{array} \right) \right). \quad (24)$$

As in Algorithm 2, by storing the Hadamard products, the procedure for computing the partial derivative of the penalty w.r.t. all factor matrices scales linearly with N rather than quadratically, leading to a time complexity of $\mathcal{O}(NR^2d)$ (see Algorithm 4). Moreover, its memory complexity is $\mathcal{O}(NRd + R^2)$. To further speed up the algorithm, it is possible to store the matrix products $\left(\mathbf{A}^{(n)} \circledast \mathbf{B} \right)^T \left(\mathbf{A}^{(n)} \circledast \mathbf{B} \right)$ in the first `for` loop to avoid computing them in the second one. This would have no effect on the asymptotic computational complexity and would increase the memory complexity to $\mathcal{O}(NRd + NR^2)$.

VIII. INITIALIZATION OF FACTOR MATRICES

One way to initialize the factor matrices is to use independent Gaussian noise, centered around 0 and with a tuned standard deviation. However, if the local feature map is of the form $\phi(x_n) = [1, \psi^{(1)}(x_n), \dots, \psi^{(d-1)}(x_n)]^T$, where $\psi^{(j)}: \mathbb{R} \rightarrow \mathbb{R}$, one can employ the solution of a linear model (linear or logistic regression depending on the task), trained on the set of features $\{\psi^{(j)}(x_n) \mid 1 \leq j \leq d-1, 1 \leq n \leq N\}$. Note that one can also train the linear model on a subset of this set, as is done in Example 4, but for clarity we assume for now the full set of transformed features.

Let b denote the bias term of the linear model trained on the aforementioned set; in addition, let $w_{n,j}$ denote its weight

Algorithm 4: Partial Derivative of Order Regularization Penalty

Input: Factor matrices $\mathbf{A}^{(n)} \in \mathbb{R}^{d \times R}$, $1 \leq n \leq N$, order regularization parameter $\mathbf{b} \in \mathbb{R}^{d \times 1}$, and regularization coefficient $\alpha \in \mathbb{R}$

Output: Partial derivative $\frac{\partial P}{\partial \mathbf{A}^{(n)}} \in \mathbb{R}^{d \times R}$ for $1 \leq n \leq N$

```

begin
   $\mathbf{B} = [\mathbf{b}, \dots, \mathbf{b}]^T \in \mathbb{R}^{d \times R}$ 
   $\mathbf{P} = [\mathbf{1}, \dots, \mathbf{1}]^T \in \mathbb{R}^{R \times R}$  // Initialize all-ones matrix
  for  $n = 1, \dots, N$  do
     $\mathbf{P} \leftarrow \mathbf{P} \otimes \left( \left( \mathbf{A}^{(n)} \otimes \mathbf{B} \right)^T \left( \mathbf{A}^{(n)} \otimes \mathbf{B} \right) \right)$  // Store
    Hadamard products
  end
  for  $n = 1, \dots, N$  do
     $\mathbf{D} = \mathbf{P} \oslash \left( \left( \mathbf{A}^{(n)} \otimes \mathbf{B} \right)^T \left( \mathbf{A}^{(n)} \otimes \mathbf{B} \right) \right) \in \mathbb{R}^{R \times R}$ 
    // Divide element-wise
     $\frac{\partial P}{\partial \mathbf{A}^{(n)}} = 2\alpha \mathbf{B} \otimes \left( \left( \mathbf{A}^{(n)} \otimes \mathbf{B} \right) \mathbf{D} \right)$ 
  end
end

```

corresponding to the n^{th} feature and the function $\psi^{(j)}$. Then, the CP-based model produces the same predictions as the linear model if the entries of the factor matrices are given by

$$\begin{aligned}
 a_{1,r}^{(n)} &= \begin{cases} \frac{b}{N}, & \text{for } r = n \\ 1, & \text{for } 1 \leq r \leq N, r \neq n, \\ 0 & \text{otherwise} \end{cases} \\
 a_{j,r}^{(n)} &= \begin{cases} w_{r,j-1}, & \text{for } r = n, j = 2, \dots, d \\ 0 & \text{otherwise} \end{cases} \quad (25)
 \end{aligned}$$

With such an initialization, the error at the first epoch tends to be lower than with random initialization and sometimes also converges to a lower point. This is especially common when the number of features is high (e.g., larger than 20).

To prove that the initialization indeed yields the same prediction as the linear model, notice from (11) that the bias term for the CP-based model is obtained through the sum of the Hadamard products of the first rows of the factor matrices. Therefore, the bias of the model equals

$$\left(\bigotimes_{k=1}^N \hat{\mathbf{a}}_1^{(k)} \right) \mathbf{1} = \underbrace{\left[\frac{b}{N}, \dots, \frac{b}{N}, 0, \dots, 0 \right]}_{N \text{ times}} \mathbf{1} = \mathbf{b}. \quad (26)$$

Moreover, the coefficient for $\psi_j(x_n)$ equals

$$\begin{aligned}
 \left(\bigotimes_{\substack{k=1 \\ k \neq n}}^N \hat{\mathbf{a}}_1^{(k)} \otimes \hat{\mathbf{a}}_{j+1}^{(n)} \right) \mathbf{1} &= \left(\underbrace{\left[\frac{b}{N}, \dots, \frac{b}{N}, 1, \frac{b}{N}, \dots, \frac{b}{N}, 0, \dots, 0 \right]}_{n-1 \text{ times}} \underbrace{\left[\frac{b}{N}, \dots, \frac{b}{N}, 0, \dots, 0 \right]}_{N-n \text{ times}} \right) \\
 &\otimes \underbrace{\left[0, \dots, 0, w_{n,j}, 0, \dots, 0 \right]}_{n-1 \text{ times}} \mathbf{1} = w_{n,j}. \quad (27)
 \end{aligned}$$

The coefficient for the second-order interaction $\psi_q(x_l)\psi_r(x_m)$ for $1 \leq q, r \leq d-1$, $1 \leq l, m \leq N$, and $l \neq m$ is

$$\left(\bigotimes_{\substack{k=1 \\ k \neq l \\ k \neq m}}^N \hat{\mathbf{a}}_1^{(k)} \otimes \hat{\mathbf{a}}_{q+1}^{(l)} \otimes \hat{\mathbf{a}}_{r+1}^{(m)} \right) \mathbf{1} = 0 \quad (28)$$

since $\hat{\mathbf{a}}_{q+1}^{(l)} \otimes \hat{\mathbf{a}}_{r+1}^{(m)} = \mathbf{0}$ for all l, m , $l \neq m$ and all q, m . Finally, following this logic, it is obvious that the coefficients of the higher-order interactions are also 0.

Example 4. A corollary is that the CP-based model with the polynomial feature map given by (16) contains the solution of the linear model trained on the original features. Namely, given the coefficient for the n^{th} feature w_n , the relevant initialization for the entries of the factor matrices is

$$\begin{aligned}
 a_{1,r}^{(n)} &= \begin{cases} \frac{b}{N}, & \text{for } r = n \\ 1, & \text{for } 1 \leq r \leq N, r \neq n, \\ 0 & \text{otherwise} \end{cases} \\
 a_{2,r}^{(n)} &= \begin{cases} w_n, & \text{for } r = n \\ 0 & \text{otherwise} \end{cases} \quad (29)
 \end{aligned}$$

and all other rows equal $\mathbf{0}$, since they correspond to features raised to higher powers than 1.

Remark 2. When dealing with categorical features that are one-hot encoded, the initialization changes slightly due to the fact that the number of rows of the factor matrices is not constant (see Section VI). Given N categorical features, each assuming K_n ($1 \leq n \leq N$) values, the rows of the factor matrices can be initialized as in (25), except that d must be replaced with K_n . Note that in this case, $w_{n,j}$ denotes the weight of the binary feature corresponding to the n^{th} categorical feature and its j^{th} possible value.

IX. EXPERIMENTS

To demonstrate the performance and flexibility of our model on different tasks, experiments were performed on a synthetic polynomial regression task, the MovieLens 100K recommender system dataset (classification on very sparse data), and the famous California Housing dataset (regression with many outliers). The first dataset is a toy example that illustrates the effects of initialization from the linear model solution and order regularization for lower than and higher than optimal local dimensions. The MovieLens dataset shows how our model can be successfully employed for sparse (categorical) data. Finally, the utility of using very high local dimension, coupled with normalized polynomial feature mappings, is illustrated on the California Housing dataset.

We evaluated our model's performance against the TT-based model as well as other common supervised learning models. For the former, we used the code provided in Google's TensorNetwork library [24]. Moreover, we used the scikit-learn implementation of the SVM and the Keras library to construct the neural networks, as well as

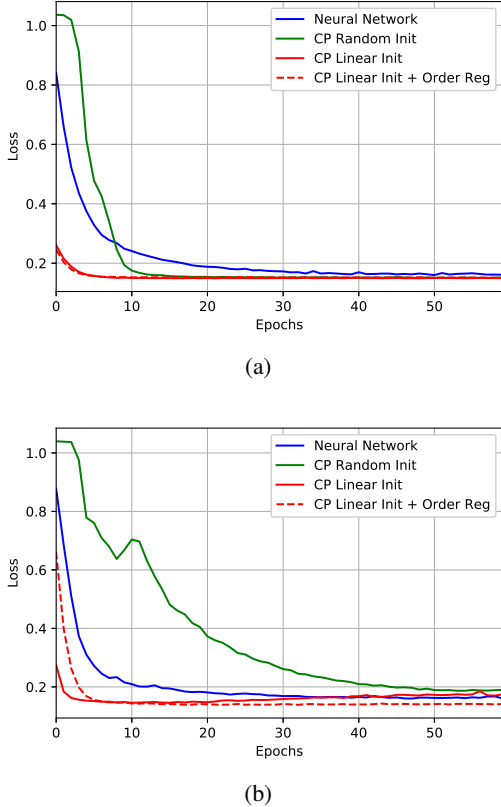


Fig. 6: Learning curves of validation MSE for the synthetic polynomial regression task. The effects of initialization with the linear model solution and order regularization are shown for a (a) smaller local dimension than optimal ($d = 2$) and $R = 7$, and (b) larger local dimension than optimal ($d = 4$) and $R = 30$.

`polylearn`³ and `tffm`⁴ for the polynomial networks and higher-order factorization machines, respectively.

A. Effects of Initialization and Order Regularization

For this experiment, the target function was set to a 2nd-order polynomial of 3,000 samples of four features with added white Gaussian noise, and the models were trained on seven features, i.e., three of the features were non-informative. We used the (unnormalized) polynomial map, so that the target function was included in the CP- and TT-based models’ hypotheses sets (for $d \geq 3$). As a preprocessing step, we standardized the features by subtracting the mean and dividing by the standard deviation. We used the mean squared error as the loss function. Moreover, for the iterative methods, the mini-batch size was set to 32, and the ADAM optimizer was used, as it performed better than plain SGD. The neural network was composed of three hidden layers, with 20 neurons for the first two and 15 for the last, all followed by ReLU activation and batch normalization [25]. 20% of the dataset was held out for testing and 20% of the remaining data points formed the validation set.

³<https://github.com/scikit-learn-contrib/polylearn>

⁴<https://github.com/geffy/tffm>

TABLE I: Validation losses and training times for the synthetic regression dataset.

Method	Val Loss	Train Time (sec)
CP-Based ($d = 3$)	0.1378	11.09
Linear Regression	0.3311	0.03
RBF SVR	0.1790	1.30
Neural Network	0.1545	20.59
3 rd -order Polynomial Network	0.1390	6.96
3 rd -order Factorization Machine	0.1485	4.35

Fig. 6 shows the influence of linear initialization and order regularization on our model for different local dimensions, with the neural network acting as a baseline. Specifically, we trained the models for 60 epochs, first with random initialization (zero-mean Gaussian noise with standard deviation of 0.2) and no regularization, then with the linear model solution as initialization, and finally we added order regularization with $\beta = 3.0$ and $\alpha = 10^{-3}$. In the top panel of the figure, we show the learning curves when $d = 2$ and $R = 7$, i.e., the model was not expressive enough to capture the 2nd-order terms of the polynomial. Despite the linear-initialized model starting from a significantly lower validation error and converging faster, both initialization schemes led to the model reaching the same error after 4-5 epochs; the neural network converged after about 60 epochs to a similar value. Also, order regularization did not have a significant effect on the performance of the model. On the other hand, when d was increased to four (a higher than optimal local dimension, as there were no 3rd-order terms) and R to 30, random initialization took significantly longer to converge (around 60 epochs, then it started overfitting), whereas order regularization enabled the optimization procedure to reach a lower validation error.

The comparison with the other models is given in Table I, where the minimum validation score across 100 epochs is reported. We were not able to run the TT-based models with the unnormalized polynomial mapping (neither Google’s TensorNetwork nor Exponential Machines with $d = 2$), as the loss diverged with all hyperparameters we tried.

B. Performance on Recommender System

Categorical data cause issues to traditional neural networks and SVMs due to data sparsity after one-hot encoding. For example, SVMs with a polynomial kernel find it difficult to learn the coefficients corresponding to interactions of two or more categorical features, because there are usually not enough training points where the relevant binary, one-hot features are both “hot.” In contrast, the CP-based model factorizes these coefficients and, thus, performs well in such settings (for a detailed discussion on why factorized models perform well with sparse data see [26]).

We demonstrate the performance of our model on the MovieLens 100K, a widely-used benchmark for sparse data classification. For details on the dataset, see [27]. For the preprocessing of the data, we followed the procedure described in [13], in order to be able to directly compare the results with the TT-based model (Exponential Machines). The features were mapped as described in Section VI-C. The CP rank was set to 30, and order regularization was added with $\beta = 3.6$

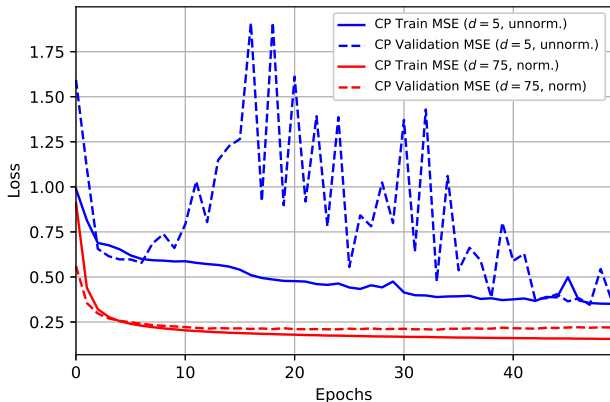


Fig. 7: Learning curves for $d = 5$ with the unnormalized polynomial map and for $d = 75$ with the normalized polynomial map.

and $\alpha = 5 \times 10^{-5}$, respectively. We trained the model until convergence, obtaining an Area Under Curve (AUC) score of 0.7863. The authors of Exponential Machines reported an AUC score of 0.784, and we could not achieve a higher score by tuning their model. Note that logistic regression obtains a score of 0.7821. For a comparison with other models, we refer the reader to [13]. We found that both initialization from the linear model solution and order regularization helped significantly in achieving better performance on this task.

C. Effect of Local Dimension

We now show the effect of high d on a common regression dataset. The California Housing dataset is a single-target regression task, comprising eight features and 20,640 samples. We performed similar data pre-processing for this experiment as for the synthetic example. The CP rank was set to 20. We found that, for the polynomial map, increasing d from two to three boosted performance, but any increase thereafter caused the learning procedure to be highly unstable and eventually to experience numerical overflow. Standardizing (zero mean, unit standard deviation) each element of the resulting vector after mapping prevented overflow but led to relatively erratic learning curves for validation (see Fig 7).

In contrast, the model with the normalized polynomial map (with random initialization⁵) was able to be trained reliably even for very high d , as can be seen from the smooth learning curves in Fig. 7. In addition, the training error kept decreasing to very small values without regularization, reflecting the gains in expressiveness (see Fig. 8). More surprisingly, however, the lowest validation error (without regularization) was obtained with $d = 25$, and it remained low even for dimensions around 100, indicating the regularization capabilities of low rank. Of course, with a smaller dataset, we would observe more overfitting for high d . With L2 regularization on the factor matrices, it reached its smallest value at $d = 75$ (we did not observe any improvement using order regularization over L2 with this map and on this dataset).

⁵One could also use initialization from the linear model.

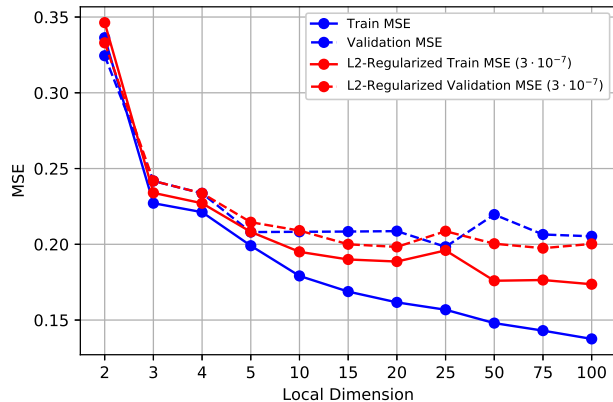


Fig. 8: Validation loss as a function of the local dimension with and without L2 regularization.

TABLE II: Validation losses and training times for the California Housing dataset.

Method	Val MSE	Train Time (sec)
CP-Based ($d = 2$, unnorm.)	0.3348	36.40
CP-Based ($d = 5$, unnorm.)	0.4221	41.29
CP-Based ($d = 25$, norm.)	0.2090	51.15
CP-Based ($d = 75$, norm., w/ L2)	0.1959	118.84
TT-Based ($d = 25$, norm.)	0.2139	773.25
Linear Regression	0.3712	0.01
RBF SVR	0.2236	18.78
Neural Network	0.2029	153.20
4th order Polynomial Network	0.2761	9.06
4th order Factorization Machine	0.3322	51.69

Not only does higher d result in great gains in performance, but due to optimized matrix-vector multiplications in TensorFlow, high d also has a small impact on training time, enabling fast tuning of this hyperparameter (see Fig. 9).

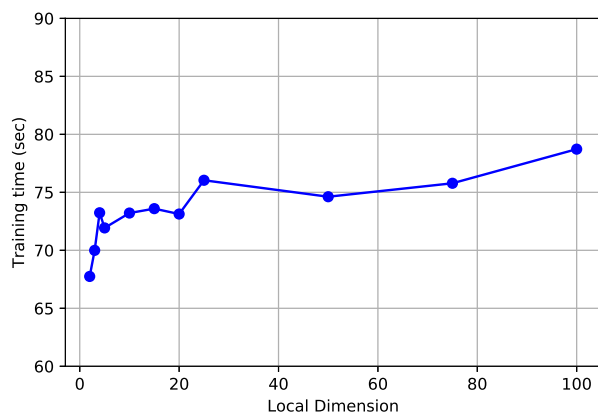


Fig. 9: Training time in seconds as a function of the local dimension (run for 50 epochs and CP rank equal to 20).

The comparison with the other models is given in Table II. As there is currently no implementation of Exponential Machines with Riemannian optimization for high d , we used the TensorNetwork library to compare with a TT-based model. The TT rank was set to 5, leading to the same number of

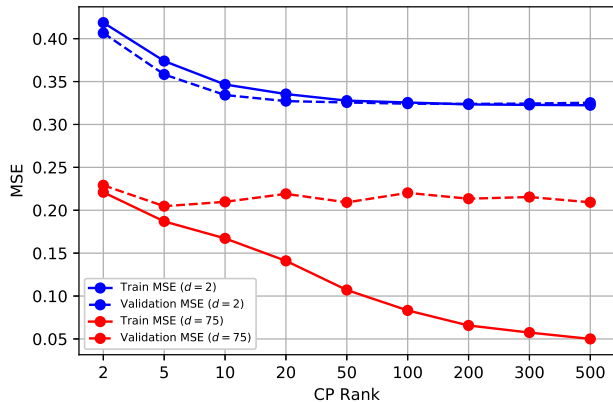


Fig. 10: Training and validation losses as functions of the CP rank for low and high local dimensions.

parameters as the CP-based model. The number of parameters for the TT-based model is $2dR_{\text{TT}} + (N - 2)dR_{\text{TT}}^2$, while for the CP-based model it is NdR , where R_{TT} is the TT rank. For $N = 8$, $R_{\text{TT}} = 5$ corresponds to $R = 20$. Note that the very large training time compared to the CP-based model is likely due to the different implementation in TensorFlow, and not due to the TT-based model being inherently slower to train for the same number of parameters. The feedforward neural network that we constructed contained four hidden layers and also had an equal number of parameters. The minimum validation score across 100 epochs is reported.

D. Effect of CP Rank

The CP rank seems to affect performance differently for low d than for high. As can be seen in Fig. 10, both the training and validation errors were decreasing up to rank equal to 50 and then plateaued for $d = 2$. On the other hand, when d was increased to 75, although the training error was decreasing with higher rank, the validation error remained fairly constant. Notice that even with very small rank (about 2 to 5), the validation error still managed to stay dramatically lower than for any value of rank with $d = 2$. This suggests that the local dimension is more important than the rank for accurate model predictions. Finally, low validation error is observed even when the rank was set to larger values (e.g., 500) in the case with $d = 75$.

E. Effect of Large Number of Features

Increasing the number of features beyond a certain point (e.g., about 30) often makes the optimization process more sensitive to the standard deviation of the Gaussian distribution, assuming random initialization is used. This phenomenon is due to the many Hadamard products (or matrix-matrix products in the case of TT-based models) that are performed: if the standard deviation is too small or too big, this can lead to vanishingly small or exceedingly large predictions, respectively. Initialization with any linear model solution (not necessarily a linear model trained on the dataset at hand) largely alleviates

this issue, as was confirmed when we managed to train a model on the (flattened) MNIST dataset with 784 features. It would be interesting to investigate other strategies that could enable these models to achieve state-of-the-art results on very high-dimensional datasets.

X. RELATED WORKS

In this section, we discuss similarities and differences between the CP-based model and related works.

A. TT-based Models

Both [12] and [13] used the TT format to limit the model parameters. The former proposed an algorithm inspired from quantum physics that allows the adaptation of the TT rank during training; unfortunately, it scales cubically with the local dimension d . The latter group designed a stochastic version of a Riemannian optimization approach, which they found to be more robust to initialization than stochastic gradient descent methods. In terms of the local feature mappings, both works used $d = 2$ (see Section VI).

To better understand how the TT-based models are linked to the CP-based one, it is worthwhile to notice that a CP decomposition can be expressed in terms of the TT format. Specifically, a tensor in the CP format with rank R is equivalent to a tensor in the TT format, for which the TT cores are given by $\mathcal{G}^{(1)} = \mathbf{A}^{(1)}$, $\mathcal{G}^{(N)} = \mathbf{A}^{(N)T}$, and $\mathbf{G}_{i_n}^{(n)} = \text{diag}(a_{i_n,1}, \dots, a_{i_n,R})$ for $n = 2, \dots, N - 1$, where $\mathbf{G}_{i_n}^{(n)}$ are the lateral slices of the cores [28]. Hence any CP-decomposed weight tensor can be converted into its TT format. However, the predictions produced by the models are not equivalent, since an optimization process on the TT-based model alters the off-diagonal terms, i.e., they are not constrained to be zero. Thus, differences in performance between the two models must arise due to off-diagonal core elements either being helpful or detrimental to generalization capabilities for the dataset at hand. Viewed another way, for equal number of parameters, the TT-based model will achieve superior results if and only if it is better for generalization to have TT cores whose slices are relatively small matrices with off-diagonal terms rather than larger diagonal matrices. Note also that any tensor in the TT format can be mapped to a tensor in the CP format, but, in general, the CP rank equals $R_1 R_2 \dots R_{N-1}$, where TT rank = $\{R_1, \dots, R_{N-1}\}$ [28].

A potential advantage of the CP-based model for non-sequential data is its insensitivity to the ordering of the features, as, when constrained to be laterally diagonal, the cores can be permuted in any way without altering the decomposition (since diagonal matrices commute). By the same token, the TT-based models may be more suitable for sequential data due to the inherent ordering of their cores.

B. Kernel SVM

The CP-based model with polynomial feature map resembles in some ways an SVM with the polynomial kernel, the prediction of which is given by

$$\hat{y}(\mathbf{x}) = \langle \psi(\mathbf{x}), \mathbf{w}_{\text{svm}} \rangle, \quad (30)$$

where ψ maps the feature vector \mathbf{x} into a higher-dimensional space, and \mathbf{w}_{svm} are the parameters of the SVM model. SVM with a polynomial kernel $K(\mathbf{x}, \mathbf{z}) = \langle \psi(\mathbf{x}), \psi(\mathbf{z}) \rangle = (\langle \mathbf{x}, \mathbf{z} \rangle + 1)^i$, can model an i^{th} -degree polynomial, similarly to our model (with $d = i + 1$). The disadvantages of the polynomial SVM compared to the CP-based model, however, are that

- they scale at least quadratically with the training set size
- they tend to overfit the data for large i since, unlike our model, the model parameters are independent of each other
- they cannot effectively capture interactions for sparse (categorical) data (e.g., recommender systems)
- they are not as interpretable since one cannot recover the coefficients of the polynomial
- the prediction depends on the training data, or support vectors

C. Higher-Order Factorization Machines and Polynomial Networks

Higher-Order Factorization Machines (HOFM) [26] address the limitations of the SVMs by factorizing the interaction parameters. The order in this case refers to the highest degree of feature interactions being modelled (e.g., an order of three refers to modelling interactions containing a maximum of three variables). Although HOFM resembles the CP-based model when $\phi(x_n) = [1, x_n]^T$, there are some important differences, which can be illuminated by casting HOFM into the tensor format [29].

HOFM with order L can be expressed in this format as

$$\hat{y} = \sum_{l=1}^L \sum_{j_1 > \dots > j_l} \hat{w}_{j_1, \dots, j_l}^{(l)} \prod_{k=1}^l x_{j_k}, \quad (31)$$

where the weight tensors $\hat{W}^{(l)} \in \mathbb{R}^{N_l}$ ($l = 1, \dots, L$) are represented in the *symmetric* CP format. Furthermore, in this formulation we observe the outer product of the whole feature vector \mathbf{x} with itself L times. Finally, only the entries above the super-diagonal of the weight tensors (which correspond to the products of distinct features) are used to construct the output. In contrast, the CP-based model takes the inner product between a tensor assumed to be in the (asymmetric) CP format (and of order equal to the number of features) and a tensor formed from the outer product of the local feature maps $\phi(x_n) = [1, x_n]^T$.

Similarly, polynomial networks (PN) [30] can be cast as [29]:

$$\hat{y} = \sum_{l=1}^L \sum_{j_1, \dots, j_l} \hat{w}_{j_1, \dots, j_l}^{(l)} \prod_{k=1}^l x_{j_k}, \quad (32)$$

(the difference with (31) is in the subscript of the second sum) and is related in the same way to our model when $\phi(x) = [1, x, x^2, \dots, x^{(d-1)}]^T$.

Unlike HOFM and PN, the CP-model allows for the modelling of all-order interactions with a computational complexity that scales linearly with the number of features during both inference and training.

D. Convolutional Arithmetic Circuits

The CP-based model can be viewed as a special case of the model presented in [6] (see Section 3 in the reference). In that work, they represent a data instance as a collection of vectors, each of dimensionality s . In the case of a grayscale image, these vectors may correspond to s consecutive pixels. They then apply so-called representation functions (analogous to the local feature maps) on each of these vectors, using the example of an affine transformation followed by an activation function. They refer to this model as Convolutional Arithmetic Circuit due to the nature of their representation function. The main differences between the CP-based model and the model presented in their work are that we use $s = 1$ and the representation functions that we apply are the ones given in Section VI.

The authors proved in [6] that a model based on the Hierarchical Tucker decomposition is exponentially more expressive than one based on CP; that is, an HT-based model realizes functions that would almost always require a CP-based model with an exponentially large rank to even approximate them. A similar result was proved in [7], where they compared a model based on CP with one based on TT. Although this may at first seem like a disadvantage of the CP-based model, we argue that this is not so, at least for non-sequential data. The model architecture captures an inductive bias about the task at hand, and due to either potential overfitting or optimization difficulties, a model that is more expressive than necessary is likely to converge to a solution that is inferior to the one obtained by a model well-suited to the data. Our experiments on non-sequential data comparing CP- and TT-based models confirm this hypothesis. We also show that increasing the rank did not significantly improve the validation loss, which is further empirical evidence that it is unlikely that the target function for these tasks is one that the CP needs an exponentially large rank to approximate.

XI. CONCLUSION AND FUTURE WORK

We have presented scalable inference and learning algorithms for a supervised learning model based on the Canonical Polyadic (CP) decomposition to serve as a potential alternative to the existing methods based on the Tensor Train (TT) for non-sequential tasks. This model is applicable to both standard classification and regression tasks as well as recommender systems. We also derived efficient procedures to incorporate order regularization and showed how to initialize the model using a linear model solution. In addition, we proposed a unit-normalized version of an arbitrarily high-dimensional local feature map, which enables the straightforward increase of model expressiveness and remains stable for very high dimensions.

With regard to future research directions, it would be interesting to extend the Riemannian optimization approach of Exponential Machines to handle high local dimensions for TT-based supervised learning and compare the performance with adaptive gradient approaches. It could also be fruitful to experiment with other local feature maps and compare them with those considered in this paper. Another potential

follow-up work could be finding novel techniques to help in the training of the models when the dimensionality of the features is very high. Finally, future research could focus on the generalization ability of the models when different tensor networks (TNs) are employed to represent the weight tensor, depending on the nature of the data at hand. For example, given the inherent one-dimensional structure of natural language processing problems or the two-dimensional nature of images, it seems likely that the TT representation (1-D TNs) would lead to superior performance in the former case and PEPS [31] (2-D TNs) would be more suitable in the latter case.

APPENDIX A PROOF OF KHATRI-RAO PROPERTY

We prove here the identity in (1). Let $\mathbf{A}^{(k)} \in \mathbb{R}^{I_k \times J}$ and $\mathbf{B}^{(k)} \in \mathbb{R}^{I_k \times L}$, $1 \leq k \leq N$. Since

$$\begin{aligned} \left(\bigcirc_{k=1}^N \mathbf{A}^{(k)} \right)^T &= \left[\bigotimes_{k=1}^N \mathbf{a}_1^{(k)} \quad \cdots \quad \bigotimes_{k=1}^N \mathbf{a}_J^{(k)} \right]^T, \\ \left(\bigcirc_{k=1}^N \mathbf{B}^{(k)} \right) &= \left[\bigotimes_{k=1}^N \mathbf{b}_1^{(k)} \quad \cdots \quad \bigotimes_{k=1}^N \mathbf{b}_L^{(k)} \right], \end{aligned}$$

and using the mixed-product property [32]

$$\left(\bigotimes_{k=1}^N \mathbf{a}_j^{(k)T} \right) \left(\bigotimes_{k=1}^N \mathbf{b}_j^{(k)} \right) = \bigotimes_{k=1}^N \mathbf{a}_j^{(k)T} \mathbf{b}_j^{(k)} \quad (33)$$

we get

$$\begin{aligned} &\left(\bigcirc_{k=1}^N \mathbf{A}^{(k)} \right)^T \left(\bigcirc_{k=1}^N \mathbf{B}^{(k)} \right) \\ &= \begin{bmatrix} \bigotimes_{k=1}^N \mathbf{a}_1^{(k)T} \mathbf{b}_1^{(k)} & \cdots & \bigotimes_{k=1}^N \mathbf{a}_1^{(k)T} \mathbf{b}_L^{(k)} \\ \vdots & \ddots & \vdots \\ \bigotimes_{k=1}^N \mathbf{a}_J^{(k)T} \mathbf{b}_1^{(k)} & \cdots & \bigotimes_{k=1}^N \mathbf{a}_J^{(k)T} \mathbf{b}_L^{(k)} \end{bmatrix} \\ &= \begin{bmatrix} \prod_{k=1}^N \mathbf{a}_1^{(k)T} \mathbf{b}_1^{(k)} & \cdots & \prod_{k=1}^N \mathbf{a}_1^{(k)T} \mathbf{b}_L^{(k)} \\ \vdots & \ddots & \vdots \\ \prod_{k=1}^N \mathbf{a}_J^{(k)T} \mathbf{b}_1^{(k)} & \cdots & \prod_{k=1}^N \mathbf{a}_J^{(k)T} \mathbf{b}_L^{(k)} \end{bmatrix} \\ &= \bigcirc_{k=1}^N \mathbf{A}^{(k)T} \mathbf{B}^{(k)}. \end{aligned} \quad (34)$$

APPENDIX B PROOF OF MATRIX CALCULUS IDENTITY

We prove here the identity in (23). Let $\mathbf{Y} = \mathbf{X} \circledast \mathbf{W}$ and a colon ($:$) denote the inner product operator. Then,

$$\begin{aligned} q &= \text{Tr} \left(\mathbf{Y} \mathbf{Z} \mathbf{Y}^T \right) \\ &= \text{Tr} \left(\mathbf{Y}^T \mathbf{Y} \mathbf{Z} \right) \\ &= \mathbf{Z} : \mathbf{Y}^T \mathbf{Y}. \end{aligned} \quad (35)$$

We obtain the differential:

$$\begin{aligned} dq &= \mathbf{Z} : d(\mathbf{Y}^T \mathbf{Y}) \\ &= \mathbf{Z} : \mathbf{Y}^T d\mathbf{Y} + d\mathbf{Y}^T \mathbf{Y} \\ &= \mathbf{Z} : \mathbf{Y}^T d\mathbf{Y} + \mathbf{Z} : d\mathbf{Y}^T \mathbf{Y} \\ &= \mathbf{Z} : \mathbf{Y}^T d\mathbf{Y} + \mathbf{Z}^T : \mathbf{Y}^T d\mathbf{Y} \\ &= \mathbf{Z} + \mathbf{Z}^T : \mathbf{Y}^T d\mathbf{Y} \\ &= \mathbf{Y} \left(\mathbf{Z} + \mathbf{Z}^T \right) : d\mathbf{Y} \\ &= \mathbf{Y} \left(\mathbf{Z} + \mathbf{Z}^T \right) : \mathbf{W} \circledast d\mathbf{X} \\ &= \left(\mathbf{Y} \left(\mathbf{Z} + \mathbf{Z}^T \right) \right) \circledast \mathbf{W} : d\mathbf{X}. \end{aligned} \quad (36)$$

Finally, this implies that

$$\frac{\partial q}{\partial \mathbf{X}} = \left(\left(\mathbf{X} \circledast \mathbf{W} \right) \left(\mathbf{Z} + \mathbf{Z}^T \right) \right) \circledast \mathbf{W}. \quad (37)$$

ACKNOWLEDGMENTS

The authors would like to thank Giuseppe Calvi and Bruno Scalzo Dees for helpful discussions. A.H. is supported by an Imperial College London President's Scholarship. K.K. is supported by an International Doctoral Scholarship provided by EPSRC.

REFERENCES

- [1] I. V. Oseledets, "Tensor-train decomposition," *SIAM Journal on Scientific Computing*, vol. 33, no. 5, pp. 2295–2317, 2011.
- [2] W. Hackbusch and S. Kühn, "A new scheme for the tensor representation," *Journal of Fourier analysis and applications*, vol. 15, no. 5, pp. 706–722, 2009.
- [3] A. Graves, A.-r. Mohamed, and G. Hinton, "Speech recognition with deep recurrent neural networks," in *2013 IEEE international conference on acoustics, speech and signal processing*. IEEE, 2013, pp. 6645–6649.
- [4] D. P. Mandic and J. Chambers, *Recurrent neural networks for prediction: learning algorithms, architectures and stability*. John Wiley & Sons, Inc., 2001.
- [5] A. Krizhevsky, I. Sutskever, and G. E. Hinton, "Imagenet classification with deep convolutional neural networks," in *Advances in neural information processing systems*, 2012, pp. 1097–1105.
- [6] N. Cohen, O. Sharir, and A. Shashua, "On the expressive power of deep learning: A tensor analysis," in *Conference on Learning Theory*, 2016, pp. 698–728.
- [7] V. Khrulkov, A. Novikov, and I. Oseledets, "Expressive power of recurrent neural networks," in *International Conference on Learning Representations*, 2018. [Online]. Available: <https://openreview.net/forum?id=S1WRibb0Z>
- [8] V. Khrulkov, O. Hrinchuk, and I. Oseledets, "Generalized tensor models for recurrent neural networks," *arXiv preprint arXiv:1901.10801*, 2019.
- [9] G. G. Calvi, A. Moniri, M. Mahfouz, Z. Yu, Q. Zhao, and D. P. Mandic, "Tucker tensor layer in fully connected neural networks," *arXiv preprint arXiv:1903.06133*, 2019.
- [10] A. Novikov, D. Podoprikin, A. Osokin, and D. P. Vetrov, "Tensorizing neural networks," in *Advances in neural information processing systems*, 2015, pp. 442–450.
- [11] W. Wang, Y. Sun, B. Eriksson, W. Wang, and V. Aggarwal, "Wide compression: Tensor ring nets," in *Proceedings of the IEEE Conference on Computer Vision and Pattern Recognition*, 2018, pp. 9329–9338.
- [12] E. Stoudenmire and D. J. Schwab, "Supervised learning with tensor networks," pp. 4799–4807, 2016. [Online]. Available: <http://papers.nips.cc/paper/6211-supervised-learning-with-tensor-networks.pdf>
- [13] A. Novikov, M. Trofimov, and I. Oseledets, "Exponential machines," *Bulletin of the Polish Academy of Sciences. Technical Sciences*, vol. 66, no. 6, 2018.

- [14] C. Guo, Z. Jie, W. Lu, and D. Poletti, "Matrix product operators for sequence-to-sequence learning," *Phys. Rev. E*, vol. 98, p. 042114, Oct 2018. [Online]. Available: <https://link.aps.org/doi/10.1103/PhysRevE.98.042114>
- [15] A. Cichocki, D. Mandic, L. De Lathauwer, G. Zhou, Q. Zhao, C. Caiafa, and H. A. PHAN, "Tensor decompositions for signal processing applications: From two-way to multiway component analysis," *IEEE Signal Processing Magazine*, vol. 32, no. 2, pp. 145–163, March 2015.
- [16] T. G. Kolda and B. W. Bader, "Tensor decompositions and applications," *SIAM Review*, vol. 51, no. 3, pp. 455–500, September 2009.
- [17] A. Cichocki, N. Lee, I. Oseledets, A.-H. Phan, Q. Zhao, and D. Mandic, "Tensor networks for dimensionality reduction and large-scale optimization: Part 1 low-rank tensor decompositions," *Foundations and Trends in Machine Learning*, vol. 9, pp. 249–429, 01 2016.
- [18] J. D. Carroll and J.-J. Chang, "Analysis of individual differences in multidimensional scaling via an n-way generalization of eckart-young decomposition," *Psychometrika*, vol. 35, no. 3, pp. 283–319, 1970.
- [19] R. Harshman, "Foundations of the parafac procedure: Models and conditions for an "explanatory" multimodal factor analysis," 1970.
- [20] M. H. Stone, "Applications of the theory of boolean rings to general topology," *Transactions of the American Mathematical Society*, vol. 41, no. 3, pp. 375–481, 1937.
- [21] D. Kingma and J. Ba, "Adam: A method for stochastic optimization," *International Conference on Learning Representations*, 12 2014.
- [22] F. Chollet *et al.*, "Keras," <https://github.com/fchollet/keras>, 2015.
- [23] D. Liu, S.-J. Ran, P. Wittek, C. Peng, R. B. García, G. Su, and M. Lewenstein, "Machine learning by unitary tensor network of hierarchical tree structure," *New Journal of Physics*, vol. 21, no. 7, p. 073059, jul 2019. [Online]. Available: <https://doi.org/10.1088>
- [24] S. Efthymiou, J. Hidary, and S. Leichenauer, "Tensornetwork for machine learning," *CoRR*, vol. abs/1906.06329, 2019. [Online]. Available: <http://arxiv.org/abs/1906.06329>
- [25] S. Ioffe and C. Szegedy, "Batch normalization: Accelerating deep network training by reducing internal covariate shift," 2015, pp. 448–456. [Online]. Available: <http://jmlr.org/proceedings/papers/v37/ioffe15.pdf>
- [26] S. Rendle, "Factorization machines," in *2010 IEEE International Conference on Data Mining*. IEEE, 2010, pp. 995–1000.
- [27] F. M. Harper and J. A. Konstan, "The movielens datasets: History and context," *ACM Trans. Interact. Intell. Syst.*, vol. 5, no. 4, pp. 19:1–19:19, Dec. 2015. [Online]. Available: <http://doi.acm.org/10.1145/2827872>
- [28] A.-H. Phan, A. Cichocki, I. Oseledets, G. G. Calvi, S. Ahmadi-Asl, and D. P. Mandic, "Tensor networks for latent variable analysis: Higher order canonical polyadic decomposition," *IEEE transactions on neural networks and learning systems*, 2019.
- [29] M. Blondel, M. Ishihata, A. Fujino, and N. Ueda, "Polynomial networks and factorization machines: New insights and efficient training algorithms," in *International Conference on Machine Learning*, 2016, pp. 850–858.
- [30] R. Livni, S. Shalev-Shwartz, and O. Shamir, "On the computational efficiency of training neural networks," in *Advances in neural information processing systems*, 2014, pp. 855–863.
- [31] G. Evenbly and G. Vidal, "Tensor network states and geometry," *Journal of Statistical Physics*, vol. 145, no. 4, pp. 891–918, 2011.
- [32] H. Zhang and F. Ding, "On the kronecker products and their applications," *J. Appl. Math.*, vol. 2013, p. 8 pages, 2013. [Online]. Available: <https://doi.org/10.1155/2013/296185>